ISTITUTO NAZIONALE DI RICERCA METROLOGICA
Repository Istituzionale

Al- and Ga-Doped TiO2, ZrO2, and HfO2: The Nature of O 2p Trapped Holes from a Combined Electron Paramagnetic Resonance (EPR) and Density Functional Theory (DFT)

Terms of use:

This article is made available under terms and conditions as specified in the corresponding bibliographic description in the repository

(Article begins on next page)

22 November 2024

Al- and Ga-doped TiO₂, ZrO₂ and HfO₂: the Nature of O 2p Trapped Holes from a Combined EPR and DFT Study

Chiara Gionco[1], Stefano Livraghi[1], Sara Maurelli[1], Elio Giamello[1], Sergio Tosoni[2], Cristiana Di Valentin[2], and Gianfranco Pacchioni[2]

1 Dipartimento di Chimica and NIS, Università di Torino Via P. Giuria 7, 10125 Torino, Italy

2 Dipartimento di Scienza dei Materiali, Università di Milano-Bicocca Via R. Cozzi 5, 20125 Milano, Italy

ABSTRACT: The nature of hole centers in a series of MeO₂ (TiO₂, ZrO₂, HfO₂) metal oxides doped with trivalent Al or Ga ions has been investigated coupling the classic Continuous Wave Electron Paramagnetic Resonance (CW-EPR) technique with advanced density functional theory (DFT) calculations. The insertion of an aliovalent ion in the structure of the tetravalent oxides is compensated by the creation of oxygen vacancies leading to diamagnetic defective systems. The hole centers are observed by EPR after irradiation using UV frequencies (with consequent formation of an electron-hole pair) and trapping of the photogenerated electron The distortion imparted by the presence of the dopant stabilizes these centers. This generates a rich super-hyperfine structure since the dopants employed in this investigation (Al and Ga) have a non-zero nuclear spin. The DFT calculations performed on a wide set of possible hole-trapping sites occurring in the solid, allow us to identify (comparing the calculated EPR parameters of various models with experimental ones) the nature of the observed hole centers in all cases. These are always three-coordinated oxygen ions with one Al (or Ga) ion in the first coordinative sphere. As it has been observed in other cases of holes centers, the spin density associated to the unpaired electron is concentrated in an oxygen p-orbital with a modest delocalization towards the first neighboring ions.

1. Introduction

Doping of metal oxides by introducing of heteroatoms is a field of enormous importance in physics, chemistry, and materials science.[1, 2] Dopants determine the optical, magnetic, electronic and chemical properties of these materials. They may stabilize phases that are unstable in the pure material, or introduce excess electrons or holes in the electronic structure, thus altering profoundly the nature of the compound and its properties. In this work we concentrate on the doping of three MeO₂ metal oxides, namely anatase TiO₂, monoclinic and tetragonal ZrO₂, and monoclinic HfO₂, by trivalent Al and Ga atoms. Assuming that the Al or Ga dopant occupies substitutional positions in the lattice replacing the tetravalent Ti, Zr, or Hf ions, a charge imbalance is introduced in the crystal lattice. The charge can be compensated, in principle, in two ways. In the first case the replacement of Ti, Zr, or Hf with Al or Ga leads to the formation of a hole in the O 2p valence band, which is a magnetic impurity. In the second one the compensating defects are oxygen vacancies, with one vacancy compensating the introduction of two triva-

lent ions.[3] Usually, the solid system spontaneously selects between these two alternative possibilities based on the thermodynamic stability of the final system. It has to be noticed that, in the former case, unpaired electron centers (holes) are introduced into the solid while in the second one the defective systems remains diamagnetic, thus EPR silent.

Al-doped titania has been studied as a potential diluted room temperature ferromagnet.[4, 5] Also in the field of microelectronics these systems have attracted considerable attention. Thin films of Al-doped zirconia and hafnia, grown on a semiconductor substrate or on a metal electrode, are used as high-k dielectrics.[6-8] Here the presence of the dopant is assumed to be relevant for the stabilization of the cubic or tetragonal phases which exhibit a higher dielectric constant. Al-doped ZrO₂ has been investigated also for logic devices and for resistive memories. More traditional areas where Al or Ga impurities have been introduced in titania are those of catalysis [9] and photo-catalysis [10-13] or in the design of dye-sensitized solar cells.[14] The purpose is that to increase the surface activity

1

of the oxides or to enhance the capture of solar light for photo-induced processes, thanks to the presence of the dopants.

The synergy between the experiment and first principle computations is a key aspect in this research field, in particular for the detailed understanding of the nature of the systems.[15, 16] As introduced above, in this study we have investigated pure and Al or Ga-doped titania, zirconia and hafnia. It will be shown in the following that these systems are diamagnetic. However, under illumination, the formation of paramagnetic defects (electron and hole centers, respectively) occurs via charge separation. We characterize the hole centers, that typically localize on oxygen ions, by a combined use of Electron Paramagnetic Resonance (EPR) Spectroscopy and Density Functional Theory (DFT). The trivalent dopants are introduced by chemical synthesis into anatase TiO_2, a semiconductor with optical band gap of 3.4 eV,[17] or monoclinic ZrO_2 and HfO_2, characterized by larger band gaps of 5-6 eV.

The correct description with theoretical methods of the band gap in semiconducting or insulating materials is a prerequisite in order to reproduce accurately the effect of the dopant on the electronic structure and properties. Local and semilocal DFT or Hartree-Fock (HF) calculations either severely underestimate or overestimate, respectively, the electronic band gap. Several studies in recent years have shown that hybrid exchange-correlation functionals, making use of a combination of exact (as in HF) and DFT exchange terms, represent a practical solution to reproduce the experimental band gap.[18] This is the approach followed here. In particular, we used the unscreened B3LYP exchange-correlation functional with 20% exact exchange.[19, 20] Amongst hybrid functionals, B3LYP has the advantage of providing a generally acceptable description of the Kohn-Sham band gap and allowing the comparison of a large database of molecular and solid state systems computed at this level. Still, the theoretical description of hole centers in the O 2p states of oxide materials is all but simple.

The localization of the hole on a specific O 2p orbital depends on the level of treatment used. The typical case where this problem becomes pathologic is that of Al-doped SiO_2.[21-24] Here standard DFT approaches predict a fully delocalized hole in disagreement with experimental evidence. Even the introduction of a portion of exact exchange as in the B3LYP approach is not sufficient to cure the problem, as the hole may remain delocalized. It is only when larger portions of exact exchange are used, above 50%, that a correct solution is obtained with a fully localized hole on an O 2p non-bonding orbital. This problem has become a classic test of the validity of a given computational approach to describe localized holes and electrons in SiO_2 and other insulators. Unfortunately, the predictive power of theory in this respect is limited as it is not possible to know "a priori" the level of correction that is required to remove the self-interaction problem. This holds true also here where Al- and Ga-doped titania, zirconia, and hafnia are considered. In ultimate analysis, only the direct comparison with the experiment provides a validation of the approach used. As we will show below,

for the materials under scrutiny it appears that the use of the B3LYP hybrid functional is fully adequate.

EPR is a key technique for the spectroscopic characterization of very small amounts of paramagnetic centers, being able to detect 10^{10} spins.[25, 26] For a complete characterization of the defects, however, a comparison with other spectroscopies or with computed spin properties is often very useful. Key quantities in EPR spectra are the **g**-tensor and the hyperfine coupling constants (*hfcc*) which provide a powerful tool to define the level of spin localization. In the case of hole centers formation, the hyperfine coupling constants with the magnetically active nucleus ^{17}O can be investigated only in samples prepared with an oxygen atmosphere enriched with this isotope. However, the interaction of the unpaired electron residing in an O 2p orbital with the first neighbor (in our case ^{27}Al or ^{69}Ga and ^{71}Ga nuclides) provides additional information about the spin distribution via the analysis of the super-hyperfine interaction. Additionally, it has been found, in the case of Al-doped SiO_2,[21] that Al super-hyperfine parameter is sensitive to the degree of localization of the hole on the nearby trapping oxygen. This interaction will be used in the following to discuss spin properties of Al-doped and Ga-doped materials. The hyperfine spin-Hamiltonian, $H_{hfc} = \mathbf{S} \cdot \mathbf{A} \cdot \mathbf{I}$, is given in terms of the hyperfine matrix **A** which describes the coupling of the electron with the nuclear spin. The components of **A** can be represented as:

$$\mathbf{A} = \begin{bmatrix} A_1 & 0 & 0 \\ 0 & A_2 & 0 \\ 0 & 0 & A_3 \end{bmatrix} = a_{iso}\mathbf{U} + \begin{bmatrix} T_1 & 0 & 0 \\ 0 & T_2 & 0 \\ 0 & 0 & T_3 \end{bmatrix} \qquad (1)$$

where **U** is the unit matrix. The isotropic part, a_{iso}, of the coupling constant is related to the spin density at the nucleus (the Fermi contact term) while the *T* matrix represents the dipolar interaction between the unpaired electron and the magnetic nucleus.

The paper is organized as follows. First the experimental procedures and the computational details are described in Section 2. Then, the EPR spectra of hole centers recorded after irradiation of the various bare and doped MeO_2 systems will be discussed, paying particular attention to the structure of the **g** tensor and to the super-hyperfine interaction with the dopant (Al, Ga) nuclei (Section 3). The successive section (Section 4) compares the experimental results with the theoretical calculations and presents a detailed description of the hole centers in all the six systems here considered. The main results are summarized in the concluding Section 5.

2. Experimental and computational details

2.1 Samples preparation.

Titanium (VI) isopropoxide 97%, Zirconium butoxide 97% and Hafnium isopropoxide 99.9% were used as precursor for Ti, Zr and Hf oxides, respectively. $AlCl_3$ and $GaCl_3$ were employed to introduce the dopant in the three oxides in order to achieve a nominal molar doping of 5%. All reactants were purchased from Sigma Aldrich Company and were employed without any further treatment.

Table 1. Experimental conditions adopted for the preparation and phase composition of the examined samples.

Sample	Calcination temperature	Calcinations time	Phase composition
TiO$_2$	773 K	2h	100% Anatase
Al-TiO$_2$	773 K	2h	100% Anatase
Ga-TiO$_2$	773 K	2h	100% Anatase
ZrO$_2$	1273 K	48h	100% Monoclinic
Al-ZrO$_2$	1273 K	48h	100% Monoclinic
Ga-ZrO$_2$	1073 K	8h	84% Tetragonal 16% Monoclinic
HfO$_2$	1173 K	2h	100% Monoclinic
Al-HfO$_2$	1173 K	2h	100% Monoclinic

In the case of TiO$_2$ and ZrO$_2$ samples, an alcoholic solution was obtained diluting the metal alkoxide in the corresponding alcohol (volume ratio 1:1). These solutions were successively hydrolizated using H$_2$O (volume ratio between alcoholic solution and H$_2$O 3.5:1). The product was left ageing overnight at room temperature and subsequently dried at 333 K until a complete drying. The dried material was eventually calcined in air (calcination details specified in Table 1).

In the case of HfO$_2$, 1.0 g of the metal alkoxide was dispersed in 50 ml of the corresponding alcohol and successively H$_2$O was added at the suspension under continuous stirring (volume ratio between alcoholic dispersion and H$_2$O 10:1). The suspension so obtained was heated at 423 K under continuous stirring until a completed removal of the solvent. The product was dried at 333 K. The dried material was eventually calcined in air (calcination details specified in Table 1).

The doped materials were obtained introducing the dopant element prior to the hydrolyzing step of the synthesis.

2.2 Spectroscopic characterization.

XRD spectra were collected on a diffractometer (PW3020, Phillips) using Cu (Kα) radiation. The phase composition obtained for each sample is listed in Table 1.

X-band Continuous Wave (CW) EPR spectra have been recorded on a Bruker EMX spectrometer equipped with a cylindrical cavity and operating at a 100 kHz field modulation. The measurements were carried out at the liquid nitrogen temperature (77 K) in quartz cells that can be connected to a conventional high-vacuum apparatus (residual pressure < 10^{-4} mbar). EPR spectra were simulated using the Easyspin package.[27] The super-hyperfine constants related to the interaction with Ga nuclei were calculated for the most abundant isotope ([69]Ga).

Trapped holes were generated upon *in situ* irradiation of the samples at T = 77K into the EPR cavity using a 1600W Xe Lamp (New Port Instruments) equipped with a IR water filter.

2.3 Computational Details.

The periodic spin-polarized calculations were carried out within the linear combination of atomic orbitals (LCAO) approach and using the B3LYP [19, 20] hybrid functional, as implemented in CRYSTAL09 code.[28, 29] With this method, the computed direct band gaps (in Γ) of bulk TiO$_2$ (anatase), ZrO$_2$ and HfO$_2$ (monoclinic) are 3.89 (indirect: 3.79), 5.63 (indirect: 5.22) and 6.55 (indirect: 6.13) eV, respectively. Higher quality GW calculations give indirect band gaps of 3.8 eV for anatase,[30] 5.4 for zirconia [31] and 6.0 eV for hafnia,[32] respectively.

We used a 2√2×2√2×1, a 2×2×2 and a 2×2×2 supercell model for TiO$_2$, ZrO$_2$ and HfO$_2$, respectively. The optimized bulk lattice parameters are: for TiO$_2$ a = 3.78, c = 9.87 ; for ZrO$_2$ a = 5.25, b = 5.25, c = 5.40 and β = 99.6°; for HfO$_2$ a = 5.18, b = 5.19, c = 5,34 and β = 99.5°. The supercells volume is approximately 1000 Å^3, while the supercell content is X$_{32}$O$_{64}$ (with X=Ti, Zr, Hf). Substitutional doping at one cationic site leads to a dopant concentration close to an atomic 3%. The reciprocal space is sampled using a Γ-centered net of 8 special K-points. We adopted an 8-411 (d1) basis set for O, an all electron 8-6411(d41) basis set for Ti, while an Hay and Wadt pseudopotential together with a 311(d31) and a 411(d31) basis sets was used for Zr and Hf, respectively[33].

3. Results and discussion

3.1 Experimental Results

All samples of p-doped MeO$_2$ prepared in this work show, after the final calcination, an EPR spectrum with a flat (or nearly flat) base line. No EPR signal amenable to the presence of magnetic impurities (trapped electrons or trapped holes) is observed. As mentioned in the introduction the presence of a trivalent cation in the tetravalent sublattice generates a charge imbalance that must be compensated within the solid. A first possibility implies the formation of a number of holes equal to that of the trivalent impurities. This is what it occurs for instance in the case of Li$^+$ doped MgO[34]. In the present case one expects that the holes (if any) localize onto oxygen ions since teravalent ions (Ti^{4+}, Zr^{4+}, Hf^{4+}) by no way can host positive carriers. Such oxygen localized hole centers are easily observed by EPR spectroscopy[35] and this is not the case for the solids here investigated. However, a further possibility exists, and this is the formation of delocalized holes, but in this case the detection of the mobile hole-centers by EPR is practically impossible[36]. There are however at least two arguments to assert that no hole is present in our starting materials. The former one is that, as it will be shown in the following, when holes are formed (by irradiation) in the investigated systems they indeed have a strongly localized character. The second one is based on the propensity of zirconia and hafnia to form oxygen vacancies to compensate the introduction of low charge ionic dopants. Zirconium dioxide, in particular, when doped with Y^{3+} or Ca^{2+} ions, form a material used as ionic conductor in solid oxide fuel cells just because of its high concentration of anion vacancies.[37] Similarly, in the case of Al^{3+} doped titania, it has been already shown that the formation of vacancies is energetically favoured with respect to the isolation of holes.[12]

On the basis of the above discussed points we thus can confidently assume that the systems investigated in this work are doped oxides containing oxygen vacancies and that they can be thus represented with the following general formula:

$$Me^{4+}_{1-2x} M^{3+}_{2x} V_O^{\bullet\bullet}{}_x O^{2-}_{2-x}$$
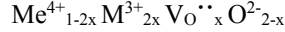
where M stays for Al or Ga and $V_O^{\bullet\bullet}$ is an oxygen vacancy indicated using the Kröger and Vink notation.

In the present study, the holes were generated by irradiation of the as prepared solids with UV photons having energy higher than their band gap. In such a case, a charge separation occurs with excitation of an electron to the conduction band and formation of a hole in the valence band.

$$MeO_2 + h\nu \rightarrow e^-_{(CB)} + h^+_{(VB)} \qquad (2)$$
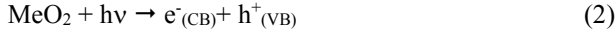
If irradiation is performed under vacuum both charge carriers can be stabilized by a cation (e$^-$) and by an oxygen anion (h$^+$) respectively. In the latter case one has:

$$h^+ + O^{2-} \rightarrow O^- \qquad (3)$$

After irradiation, the electron-hole recombination is usually slowed down keeping the solid at low temperature. In the present case, however, in order to increase the intensity of the hole signal and favor its better definition, the samples were irradiated under oxygen atmosphere at T = 77K. Oxygen in fact acts as a scavenger of photo-excited electrons forming a reduced superoxide ion (O_2^-) which remains at the surface in adsorbed state:

$$e^-_{(CB)} + O_{2\,(g)} \rightarrow O_2^-{}_{(ads)} \qquad (4)$$

Electrons, in this way, are subtracted to recombination and more intense EPR spectra of the holes are thereby observed. The interference of the EPR signal of the paramagnetic superoxide ion with that of the holes trapped in the bulk is avoided because the physisorbed molecular oxygen, covering the surface at low temperature, magnetically interacts with the adsorbed superoxide causing its spectrum to vanish.

The expected structure of the **g** tensor for the O$^-$ radical ion (electron configuration $2p_x^2$, $2p_y^2$, $2p_z^1$) has been discussed years ago by Brailsford et al.[38] In the most general case of rhombic symmetry and neglecting second order terms one has:

$$g_{zz} \approx g_e \qquad (5)$$
$$g_{xx} = g_e + 2\lambda/\Delta E_1 \qquad (6)$$
$$g_{yy} = g_e + 2\lambda/\Delta E_2 \qquad (7)$$

where λ is the spin orbit coupling constant, which for atomic oxygen amounts to 135 cm^{-1}, and ΔE_1, ΔE_2 are the energy differences corresponding to the separation between the $2p_z$ and the other two p orbitals induced by crystal field effects as shown in Scheme 1.
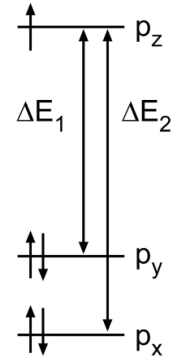
Scheme 1. Crystal field effects on a O$^-$ radical ion. Adapted from Ref. [38].

In the case of hole centers in bare MeO$_2$ oxides, the information derived from the EPR spectra are limited to the **g** tensor as ^{16}O (the dominant isotope of this element with an abundance of 99.9 %) does not generate a hyperfine structure (nuclear spin $I=0$) and therefore does not provide any information about the spin density distribution over the oxygen hole center. The same applies for the ions adjacent the hole (Ti^{4+}, Zr^{4+}, Hf^{4+}) which have no (or not enough) magnetic isotopes to origin a super-hyperfine structure capable of monitoring the spin density in the surrounding of the center. This evident drawback is the reason why, in the present work, we have employed Al- and Ga-doped oxides, both dopants having a high fraction of nuclei with $I\neq 0$. Furthermore, in this case, the holes preferentially (about 70% on average) localize on oxygen ions having one dopant ion among the nearest neighbors. This occurs because the lattice distortion, induced by the presence of the aliovalent ion, stabilizes this particular hole-site with respect to the "regular" ones (*vide infra*). For this reason the EPR spectra of doped MeO$_2$ oxides here reported are characterized by a super-hyperfine structure due a single neighboring ion (Al or Ga).

Before discussing the EPR spectra of irradiated doped materials it is useful, for sake of comparison, to briefly illustrate the features of the hole centers in the corresponding undoped samples.

3.1.1 EPR of hole centers in un-doped MeO$_2$.

The EPR spectra of a bulk hole center in the three bare oxides, namely TiO$_2$, ZrO$_2$ and HfO$_2$, are reported in Figure 1. Irradiating anatase under vacuum a quite intense EPR spectrum shows up due to the formation of trapped electrons (Ti^{3+}) and trapped hole centers (Figure 1 (a)). The EPR signal of the latter is actually due to the superposition of two distinct species respectively located at the surface and in the bulk of the oxide. The discussion of the features of the two centers is beyond the scope of the present work and will be reported in a forthcoming paper. To isolate the trace of the bulk hole centers it is however sufficient to record the EPR spectrum under oxygen at low temperature (77K). In these conditions, the trace of surface centers is smeared out by the effect of physisorbed O$_2$ while that of bulk centers remains unaffected and shows up in the spectrum of Figure 1 (a). The **g** tensor of such a signal is slightly rhombic. The values extracted from the computer simulation are listed in Table 2. Anal-

ogous spectra were obtained for ZrO_2 and HfO_2 samples (Figure 1 (b) and (c)) upon illumination in the same conditions adopted for TiO_2. Also for these oxides the EPR spectrum is dominated by a rhombic EPR pattern attributed to the generated hole on the basis of the computer simulation analysis (red lines in Figure 1, Table 2).
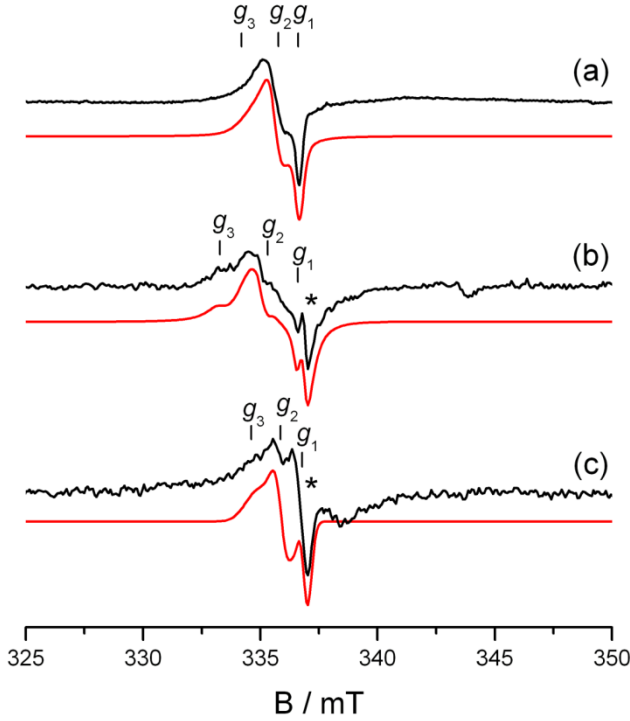
Figure 1. Experimental (black lines) and computer simulation (red lines) CW-EPR spectra of bulk hole centers in (a) TiO_2, (b) ZrO_2 and (c) HfO_2. The spectra were recorded at T = 77 K in oxygen atmosphere. The g values adopted for the computer simulations are listed in Table 2. Asterisks indicate spurious EPR signals.

3.1.2 EPR of hole centers in Al-doped and Ga-doped MeO_2.

As mentioned before, the two elements of the 3A group used to dope MeO_2 oxides are constituted exclusively by isotopes with non-zero nuclear spin, namely ^{27}Al ($I = 5/2$, Ab. 100%) and $^{69,71}Ga$ (^{69}Ga: $I = 3/2$, Ab. 60.108%; ^{71}Ga: $I = 3/2$, Ab. 39.892%). The CW-EPR spectra of the hole centers (O^-) recorded for all the samples after irradiation are reported in Figure 2.

A rather complex but well resolved EPR pattern due to the super-hyperfine interaction of the unpaired electron of the hole centers with the nuclear spin of the dopant atoms is observed for all the samples, with the exception of the Ga-HfO_2 system (*spectrum not shown*), for which only a broad unresolved absorption band has been detected. For samples doped with ^{27}Al atoms the three components of the rhombic **g** tensor of the O^- species are split in 6 hyperfine lines ($2I+1$), while in the case of the $^{69,71}Ga$ doping the hyperfine splitting consists of a 4 lines pattern for each isotope.

Table 2. Spin Hamiltonian parameters extracted from the computer simulations of the CW EPR spectra (Fig. 1 and Fig. 2) The Δg value for the various MeO_2 samples is the difference between the highest and the lowest g values of the rhombic g tensor of hole centers and it is expected to be proportional to the degree of distortion of the hole local coordination.

Oxide	Dopant	g_1	g_2	g_3	Δg (g_3-g_1)
TiO₂	-	2.005 ± 0.005	2.011 ± 0.005	2.016 ± 0.005	0.011
	Al	2.0031 ± 0.0005	2.0144 ± 0.0005	2.0265 ± 0.0005	0.023
	Ga	2.0039 ± 0.0005	2.0085 ± 0.0005	2.0258 ± 0.0005	0.022
ZrO₂	-	2.004 ± 0.005	2.015 ± 0.005	2.022 ± 0.005	0.018
	Al	2.0043 ± 0.0005	2.0168 ± 0.0005	2.0416 ± 0.0005	0.023
	Ga	1.9976 ± 0.0005	2.0142 ± 0.0005	2.0195 ± 0.0005	0.022
HfO₂	-	2.02 ± 0.01	2.01 ± 0.01	2.005 ± 0.005	0.015
	Al	2.0063 ± 0.0005	2.0158 ± 0.0005	2.0371 ± 0.0005	0.028

The computer simulation analysis of the CW EPR spectra (red lines in Figure 2) allows us to extract the spin-Hamiltonian parameters related to both **g** and **A** tensors. As it can be observed, the agreement between the experimental lines and the computer simulations is extremely satisfactory for all Al-containing samples. In the case of Ga-doped materials the fit is less good since the presence of two Ga isotopes with the same nuclear spin (3/2) but different nuclear g factor produces less resolved spectra and complicates therefore the simulation. Nonetheless, the spin-Hamiltonian parameters of the Ga doped materials can be considered more than acceptable.

Actually, in all simulations, two species have been used to fit the EPR pattern, the dominant one being characterized by a rhombic **g** tensor and by the hyperfine structure typical of the dopant atom. The second species, necessary to fit the intensity trend of the spectra, consists in the contribution of hole centers not interacting with the aliovalent element isolated in the bare oxides and examined in Figure 1. The g values extracted from the computer simulations of the spectra in Figure 2 are reported in Table 2.

*3.1.3 Structure of the **g** tensor of the hole centers*

The EPR spectra of hole centers both in bare and doped MeO_2 have a rhombic **g** tensor ($g_1 \neq g_1 \neq g_3$, Scheme 1). In

the structure of anatase the oxygen ions are tri-coordinated while in the monoclinic structures of zirconia and hafnia both tri- and tetra-coordinated sites are present. However, as it will be shown in the following, the holes tend to localize on tri-coordinated sites also in the case of the two monoclinic solids. The first information derived from the **g** tensor is that the trigonal environment around the O$^-$ ion is markedly distorted in all solids, since for a true trigonal coordination an axial structure of the tensor should be found ($g_1 = g_2 \neq g_3$). The difference from the two extreme g values of the rhombic tensor ($\Delta g = g_1 - g_3$) is a sort of indicator of the degree of rhombicity, hence of the degree of distortion of the structure.

The introduction of the dopant increases, as expected, the distortion of the environment resulting in a higher degree of g rhombicity. In the case of anatase, for example, Δg is 0.011 for the holes in the bare oxide and 0.0234 for holes in the Al-doped material. The effect of gallium is slightly weaker than that of aluminum ($\Delta g = 0.022$) due to the higher ionic radius of Ga^{3+} and the consequently lower charge/radius ratio. Similar effects are observed for zirconia and hafnia. The whole set of Δg values, monitoring the distortion of the local geometry is reported in Table 2.

3.1.4 Super-hyperfine structure of the hole centers.

The three principal values of the **A** tensor (A_1, A_2, A_3) extracted from the computer simulations are listed in Table 3.

They are quite close one to each other for all the five samples showing a resolved super-hyperfine structure. The experimental values of the Fermi contact (a_{iso}) and dipolar terms (T_1, T_2, T_3) obtained by Eq.1 are shown in Table 3 in comparison to the corresponding terms obtained from DFT calculations. A preliminary scrutiny of this tensor however clearly indicates that the involvement of the dopant nucleus (Al or Ga) in the overall spin density of the O$^-$ center is quite weak.

For example, considering in the case of Al a value of A_o = 139.55 mT for unit spin density in the 3s orbital and including a correction for departure of the average g value (g_{iso}) for O$^-$ from the free spin value (2.0023), the spin population in the Al 3s orbitals can be estimated from the following equation:

$$\rho_s = \frac{a_{iso}}{A_0} \frac{g_e}{g_{iso}} \qquad (8)$$
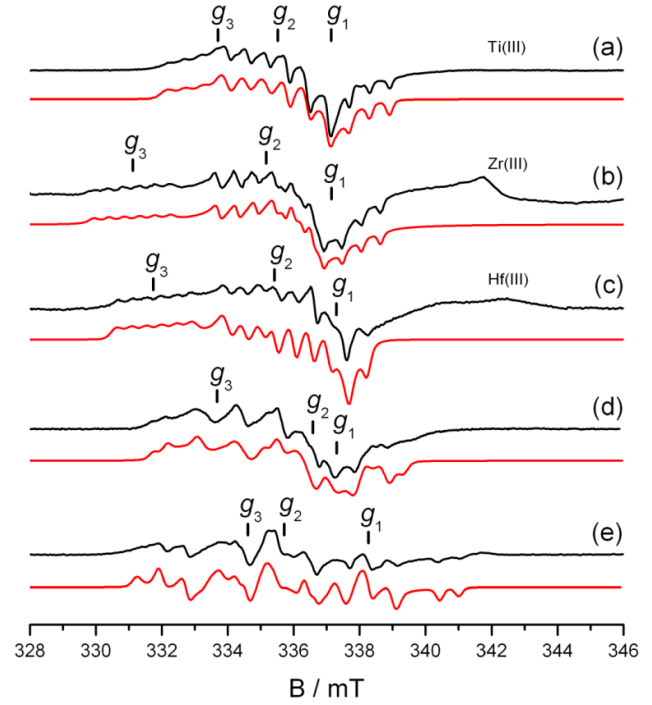
Figure 2. Experimental (black lines) and computer simulated (red lines) CW-EPR spectra of bulk hole centers in: (a) Al-doped TiO$_2$, (b) Al-doped ZrO$_2$, (c) Al-doped HfO$_2$, (d) Ga-doped TiO$_2$ and (e) Ga-doped ZrO$_2$. The spin Hamiltonian parameters adopted in the simulations are listed in Table 2 and Table 3.

Table 3. Spin Hamiltonian parameters computed from DFT calculations or extracted from the computer simulations of the experimental CW EPR spectra of Figure 2 (Exp).[1]

Oxide	Dopant		ΔE (eV)	a_{iso}	ρ_s	T_1	T_2	T_3	A_1	A_2	A_3
TiO$_2$	Al	Al$_{ax}$	+0.14	-0.348		-0.032	-0.038	+0.070	-0.380	-0.386	-0.278
		Al$_{eq}$	0.0	-0.583		-0.042	-0.040	+0.080	-0.625	-0.623	-0.503
		Exp		-0.579	0.0041	-0.027	-0.024	+0.050	-0.606	-0.603	-0.529
	Ga	Ga$_{ax}$	0.0	-1.020		-0.004	-0.003	+0.007	-1.025	-1.023	-1.013
		Ga$_{eq}$	0.0	-1.930		-0.026	-0.013	+0.039	-1.957	-1.943	-1.89
		Exp		-1.101	0.0022[2]	-0.144	+0.031	+0.114	-1.245	-1.07	-0.987
ZrO$_2$	Al	Al$_a$	0.0	-0.456		-0.034	-0.030	+0.064	-0.490	-0.490	-0.392
		Al$_b$	+0.28	-0.668		-0.044	-0.029	+0.072	-0.712	-0.696	-0.595
		Exp		-0.539	0.0039	-0.028	-0.021	+0.049	-0.567	-0.560	-0.490
	Ga	Ga$_a$	0.0	-1.650		-0.046	+0.013	+0.033	-1.695	-1.637	-1.617
		Ga$_b$	+0.24	-2.229		-0.031	-0.018	+0.049	-2.260	-2.247	-2.180

6

Oxide	Dopant	Site								
		Exp	-1.681	0.0034[2]	-0.163	-0.088	+0.250	-1.844	-1.769	-1.431
HfO_2	Al	Al_a	-0.449		-0.032	-0.029	+0.061	-0.481	-0.479	-0.388
		Exp	-0.504	0.0036	-0.037	-0.010	+0.048	-0.541	-0.514	-0.456
	Ga	Ga_a	-1.520		-0.051	+0.011	+0.039	-1.571	-1.509	-1.481

(1) The hyperfine A values are in m-Tesla. The negative sign of the Fermi contact term (a_{iso}) cannot be determined by EPR powder spectra and has been established on the basis of the computational results. a_{iso} (the Fermi contact term) and T (the dipolar tensor) are extracted from the $\mathbf{A}$ tensor. ρ_s is the spin density corresponding to the 3s and 4s orbital of Al and Ga respectively, eq. (8).

(2) Average value for the two magnetic isotopes of Gallium (^{69}Ga and ^{71}Ga).

A similar procedure can be performed for Ga but is complicated by the existence of two magnetic isotopes for this element having different A_o values. Since the hyperfine constants are very small, the experimental spectra are not fully resolved (*i.e.* there are not two independent hyperfine structures in the spectra of Ga doped materials) so that the values reported in Table 3 for Ga are less accurate than those for Al. In any case, from the whole set of data a very weak delocalization of the spin density towards the dopant orbital appears in both cases. In particular, this value is less than 0.4% for Al-doped materials and between 0.2% and 0.3% for Ga.

As for the $\mathbf{T}$ tensor values we notice that, in the case of Al, they are smaller than the expected ones estimated assuming a pure dipolar through-space interaction between the unpaired electron and the magnetic nucleus and using the Al-O calculated distance. This means that the interaction between the hole center and the neighboring ions, although very weak, is not purely dipolar and likely involves also some degree of covalency (through bond interaction).

4. Theory

4.1 Al-doped and Ga-doped anatase TiO_2

The expected quantitative level of Al^{3+} and Ga^{3+} doping in the samples investigated in the present work is 5mol%. This means that the nominal value of the molar concentration of oxygen vacancies is 2.5mol % corresponding (in the case of zirconia) to about 1 vacancy every 22 unit cells. However the losses occurring during the synthesis may lead to a smaller value of the dopant concentration. Whatever the actual degree of doping of each material the fact remains that the oxygen vacancies are rather diluted in the solid matrix. Since the holes produced by irradiation preferentially form on an oxygen ion first neighbor of a dopant (Section 3.1, Fig. 3) it is reasonable to admit that these hole centers are, on average, rather far from the anion vacancies. A theoretical model involving the presence of a vacancy in the immediate surroundings of the hole center is not therefore justified.

Table 4. Bond angles α, β and γ (in degrees) of 3-coordinated O^- sites in Al- and Ga-doped anatase TiO_2, and monoclinic ZrO_2 and HfO_2 and percentage of the spin density on the O^- site.

Oxide	Dopant	Site	α	β	γ	Spin (%)
TiO_2	Undoped	O_{3c}	153.8	103.1	103.1	-
	Al	ax	157.2	101.4	101.4	85%
		eq	164.7	97.1	98.3	87%
	Ga	ax	161.5	99.3	99.3	87%
		eq	161.4	99.9	98.7	88%
ZrO_2	Undoped	O_{3c}	145.2	104.8	110.0	-
	Al	a	140.0	97.0	122.7	89%
		b	154.0	104.3	101.7	78%
	Ga	a	140.4	99.7	119.5	88%
		b	150.9	106.1	102.9	83%
HfO_2	Undoped	O_{3c}	144.9	104.4	110.7	-
	Al	a	140.3	97.8	121.8	86%
	Ga	a	141.0	100.2	118.8	86%

The substitution of a six-coordinated Ti atom in anatase TiO_2 with Al or Ga atoms results in the formation of a hole from the valence band. At the B3LYP level, we found that the hole is localized on the 2p orbital of a three-coordinated O atom. In the anatase lattice, there are two non-equivalent O atoms. These can be classified as equatorial or axial depending on their position with respect to the Al or Ga dopant. By starting the geometry optimization from differently distorted initial structures, it has been possible to obtain the two solutions with the hole localized in different positions. As a consequence, two different super-hyperfine interactions are obtained and identified as Al_{ax} (axial) or Al_{eq} (equatorial), Table 3. The calculations show the Al_{eq} case is more stable by 0.14 eV, Table 3. In both cases the spin density is localized by 85-87% on a non-bonding O 2p orbital, Table 4.

The hole localization is accompanied by a polaronic distortion. In the undistorted TiO_2 structure the O_{3c} atom is 1.95 and 2.00 Å from the Ti ion, the α(TiOTi) angle is 153.8 degrees, and the β and γ(TiOTi) angles are 103.1 degrees respectively, Table 4. When the hole forms in the equatorial position the larger Ti-O distance elongates to 2.31 Å, while the shorter one remains almost unchanged, 1.94 Å. The other Ti-O distance becomes 2.07 Å, Figure 3. This is accompanied by an opening of the α(TiOTi) angle which becomes 164.7 degrees. In the axial case the two short Ti-O distances remain identical and slightly elon-

gated, 2.05 Å; the long distance expands from 2.00 to 2.12 Å, Figure 3.

The β and γ(TiOTi) angles remains very close to the values of the non-defective structure, Table 4. Overall, while the hole in the Al$_{eq}$ position (more stable) leads to a large polaronic distortion, very little distortion is found for the Al$_{ax}$ hole. We have also succeeded in localizing the hole on an O atom far from the dopant. However, this solution is found to be 0.18 eV higher in energy than the most stable configuration on the O adjacent to the dopant in equatorial position. The corresponding electronic structures also present some differences. In both cases the formation of a hole in the valence band results in a singly occupied α state at the top of the valence band and in an empty β component in the middle of the gap. The position of the unoccupied state, however, is different for the Al$_{ax}$ and Al$_{eq}$ cases. In particular, the hole state is 1.79 eV and 2.23 eV above the top of the VB in Al$_{ax}$ and Al$_{eq}$, respectively, Figure 4. The different structural and electronic characteristics of the two polaronic states do not reflect in a markedly different structure of the super-hyperfine tensor, Table 3. Much more relevant in this respect is the analysis of the hyperfine interaction with the ^{17}O nucleus, Table 5.

Table 5. Hyperfine DFT values of ^{17}O for Al- and Ga-doped TiO$_2$, ZrO$_2$ and HfO$_2$. Experimental values for Al-SiO$_2$ are reported for comparison. All values are expressed in mT.[(a)]

Oxide	Dopant	Spin[(b)]	a_{iso}	T_1	T_2	T_3
TiO$_2$	Al	0.87	-3.695	-8.699	4.317	4.382
	Ga	0.87	-3.679	-8.705	4.349	4.355
ZrO$_2$	Al	0.89	-3.707	-8.802	4.391	4.411
	Ga	0.88	-3.665	-8.706	4.322	4.384
HfO$_2$	Al	0.86	-3.672	-8.618	4.298	4.320
	Ga	0.86	-3.655	-8.592	4.266	4.327
SiO$_2$[(c)]	Al	-	-2.60	-8.50	4.12	4.38

(a) The values of the hyperfine tensor are listed to have $T_1 < T_2 < T_3$.

(b) Spin = spin population

(c) See refs. [21, 39, 40]
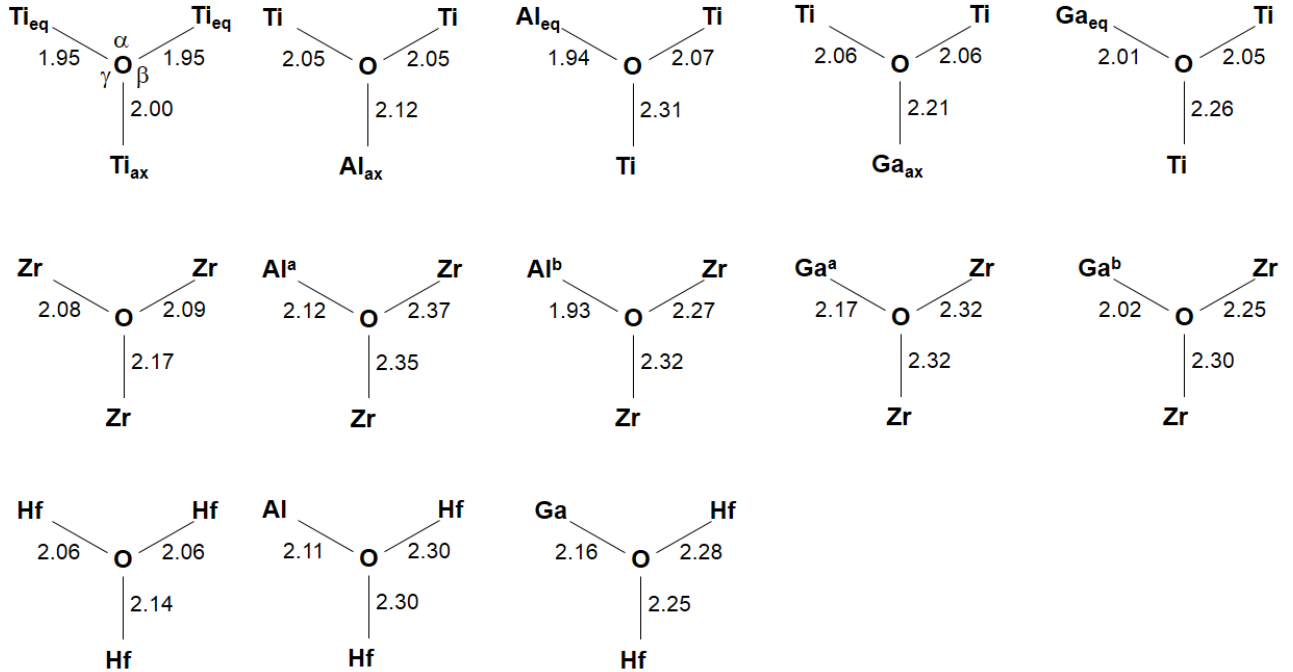
Figure 3. Bond distances (Å) at the hole site in undoped and Al- and Ga-doped TiO$_2$, ZrO$_2$ and HfO$_2$.

The picture showing up from Table 5 is that of a clear localisation of the electron spin density on the oxygen 2p orbital, similar to that found for hole centers in purely ionic systems.[41, 42] The hyperfine structure is, in this case, dominated by the dipolar term giving rise to a nearly axial **T** tensor with a minor a_{iso} component due to spin polarisation of the 2s orbital. As discussed above, there is no comparison with experiments for the data in Table 5 due to the too low natural abundance of the ^{17}O isotope.

However, we report for comparison the case of Al-doped SiO$_2$, where ^{17}O hyperfine constants have been reported.[40] The similarity with the computed values for TiO$_2$, ZrO$_2$, and HfO$_2$ is remarkable.

Coming back to the super-hyperfine structure of the Al- and Ga- doped titania, the larger Fermi contact term (a_{iso}) and the very small dipolar component suggest that the super-hyperfine interaction involves mostly the s-type orbital of the Al dopant. The comparison with the experi-

mental measurements, Table 3, shows that the computed tensor for the Al_{eq} case is clearly in better agreement, consistent with the fact that this is also the energetically more stable solution. On this basis, we propose the assignment of the observed features under irradiation to a hole localized on the Al_{eq} position.

The Ga-doped case presents some significant differences with respect to the Al-doped one. Also in this case we have been able to obtain two structurally different but isoenergetic solutions that can be classified as Ga_{ax} and Ga_{eq}, Table 3. The level of spin localization is very high in both cases, 87-88%, Table 4. The polaronic distortion of the Ga_{ax} case is quite similar to that found for Al_{ax} with the only difference of a longer Ga_{ax}-O distance, probably due to the larger size of the Ga atom compared to Al. The Ga_{eq} case is less distorted than the analogous Al_{eq} structure, Figure 3, and very similar to the Ga_{ax} polaron. Both Ga_{eq} and Ga_{ax} structures introduce an empty state in the mid of the gap of TiO_2 anatase, Figure 4. We wish to note that, as for the Al-doped case, a third configuration is possible where the hole is localized on a further apart O atom. However, this is 0.15 eV higher in energy.

The structure of the hyperfine interaction is similar as for the Al-doped case, with a very small dipolar component. The a_{iso} term is larger for the Ga_{eq} than for the Ga_{ax} case, -1.93 mT versus -1.02 mT, Table 3. This difference allows us to assign the experimentally observed signal to the presence of Ga_{ax} species.

Overall, the agreement with the experiment for Al-doped and Ga-doped anatase TiO_2 is very good, also considered that we are discussing a super-hyperfine interaction, which depends on the tails of the unpaired electron wave function.

Finally, it is interesting to note that the larger Ga dopant more nicely fits in the axial position while the smaller Al dopant prefers to lie in the equatorial site.

4.2. Al-doped and Ga-doped monoclinic ZrO_2

The local structure of monoclinic zirconia is markedly different from that of anatase. The Zr atom is coordinated to seven O atoms and the identification of an axial or an equatorial direction is no longer possible. Two non-equivalent O sites can be identified in the bulk structure, presenting different coordination: three- or four-fold. Only the three-fold coordinated O is capable of trapping the hole. Two different solutions with slightly different structural details (bond distances and angles, see Table 4) could be localized as minima on the potential energy surface. We identify these solutions as *a* and *b*, Table 3 and Table 4. In case of Al_a structure, the two Zr-O distances, around the O atom carrying the hole, are considerably elongated from 2.08-2.09 Å (undoped ZrO_2) to 2.35-2.37 Å in the doped material, Figure 3.

Also the ZrOZr angles change substantially, Table 5. The hole localization in the more stable Al_a structure is very pronounced, with a spin density of 89% on the O 2p state. The Al_b structure is 0.28 eV higher in energy and is characterized by a shorter Al-O distance, 1.93 Å compared to 2.12 Å in the Al_a case, and by ZrOZr angles closer to those of the undistorted structure. The degree of hole localization is less pronounced (78%, Table 5).

From an electronic structure point of view, we observe, as for titania, that the singly occupied α component of the O 2p orbital is just at the top of the VB, while the empty β counterpart is 1.66 eV from it for both Al_a and Al_b, Figure 4. Since the gap in ZrO_2 is much larger than in TiO_2, it follows that the state is quite deep in the gap.

With respect to Al-doped titania, Al-doped zirconia shows a similar structure of the super-hyperfine tensor, Table 3, with a dominant isotropic term and a smaller dipolar component. The structure of the tensor is very similar for Al_a and Al_b structures. A comparison with the experimentally measured tensor shows a slightly better agreement for the Al_a case, which is consistent with this structure being more stable.
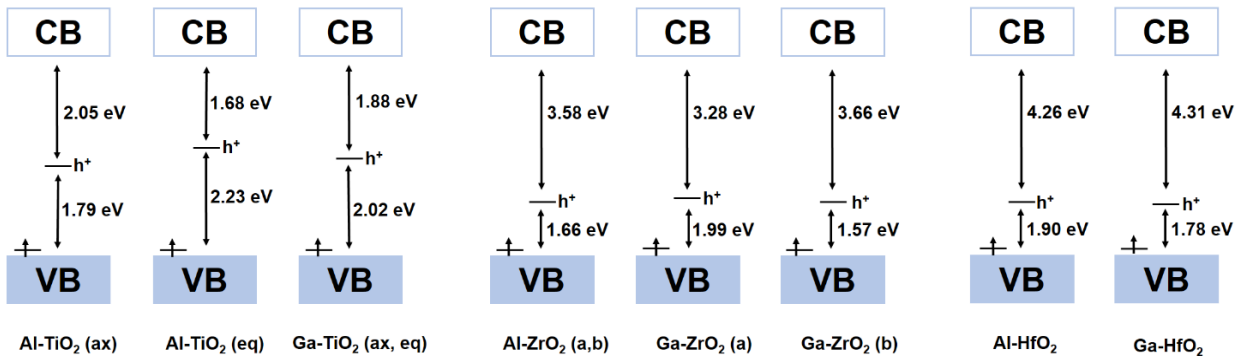
Figure 4. Schematic view of the position of the α singly occupied and β empty states in the gap of Al- and Ga-doped TiO_2, ZrO_2 and HfO_2. VB: valence band; CB: conduction band.

Also for Ga-doped zirconia it has been possible to identify two different solutions for the hole localization, identified as Ga_a and Ga_b for the similarity that these centers have with the corresponding Al_a and Al_b polarons. As for Al-doped zirconia, the Ga_a solution is more stable, exhibits a higher level of localization, and is more distorted, Table 3 and Figure 3. The two defects introduce empty β

states at 1.99 eV and 1.57 eV above the top of the VB, respectively, Figure 4.

The structure of the super-hyperfine tensor is characterized by a larger a_{iso} component and a very small dipolar part. The main difference in the hyperfine constants is that in the Ga_a case (more stable), a_{iso} = -1.65 mT, is considerably smaller than for the Ga_b structure, a_{iso} = -2.23 mT, Table 3. This difference allows a rather unambiguous assignment of the observed feature to the Ga_a species for which a_{iso} = -1.68 mT has been measured.

4. 3 Al-doped and Ga-doped monoclinic HfO$_2$

Monoclinic hafnia belongs to the same symmetry group of monoclinic zirconia, namely P2$_1$/c. Its relaxed lattice parameter is slightly shorter (5.18, 5.19 and 5.34 Å for hafnia, 5.25, 5.27 and 5.41 Å for zirconia). In both cases, the β angle is close to 99.5°. Also in this case one cannot classify the position of the O atom carrying the hole as equatorial or axial. In the case of hafnia, we have been able to find only one solution for the doped system which present analogous features as the Al$_a$ and Ga$_a$ solutions in zirconia, Figure 3 and Table 3. This seems to indicate that the second solution is unstable (several attempts have been done to obtain this second structure). With respect to the non-defective m-HfO$_2$ crystal, in Al-doped HfO$_2$ we observe a significant expansion of the Hf-O distances around the O where the hole is localized. The structure of the polaron and the level of spin localization are very similar for both Al- and Ga-doped hafnia. Also from the point view of the electronic structure the two dopants result in very similar situations. In fact, the unoccupied component of the hole state is 1.90 eV (Al) and 1.78 eV (Ga) above the top of the VB. Given the relative high band gap of crystalline HfO$_2$, 6.13 eV, the empty level lies very deep in the gap.

A comparison of computed and measured super-hyperfine interactions is possible only for the Al-case, since for Ga-doped hafnia the signal is too broad (see above). The agreement with the computed values is remarkably good, showing also in this case that the use of the B3LYP approach seems to be fully justified.

5. Conclusions

MeO$_2$ oxides (Me= Ti, Zr, Hf) when doped with the Al or Ga trivalent ions incorporate the dopant generating compensative oxygen vacancies and producing a diamagnetic solid in all cases. Centers based on hole trapping on an oxygen ion of the lattice (O$^-$) are observed upon irradiation with UV-Vis polychromatic radiation and are paramagnetic. Their EPR signals have rhombic symmetry and are dominated by a super-hyperfine interaction of the unpaired electron with the dopant nucleus while only a minor fraction of the generated hole centers concerns undoped sites. This result indicates, as also found by the calculations, that the distortion induced by the dopant ion stabilizes the hole trapping center. A comparison between experimental and DFT data has allowed the identification of the centers, although several possible structures exist. We have here explored all of them via DFT calculations and could unambiguously identify the nature of the hole trapping site among the various structural situations. In all cases, holes are strongly localized in the O

2p non bonding orbital of a three coordinated oxygen ion. The super-hyperfine interaction with the dopant ion (Al or Ga) is similar in all cases and, though producing a well resolved spectral structure, extremely weak. The propensity to the localization of the holes centers prevails on the influence of the solid nature. Strongly localized holes are observed both in ionic materials (alkaline earth oxides)[41] as well as in much more covalent ones, like silicon dioxide.[21] In Al-doped SiO$_2$ the super-hyperfine structure of an Al-O$^-$ center is extremely close to those found in this work for Al-doped TiO$_2$, ZrO$_2$, and HfO$_2$. This is based on a tiny (0.2%-0.4%) delocalization of the electron spin density towards the dopant s-orbital and on a similar interaction with the dopant p-orbitals, adding to the expected dipolar through space interaction. Given the very weak interaction of the oxygen hole centers with the surrounding cations, the analysis of the super-hyperfine interaction cannot be used to extract information about the more or less ionic or covalent nature of the host material. It also emerges from this study that in the presence of trivalent dopants, electron-hole pairs generation under illumination will result in the preferential formation of localized polaronic holes near the dopants, a fact that may affect the mobility of these species and in particular reduce it.

AUTHOR INFORMATION

Corresponding Author

* elio.giamello@unito.it

REFERENCES

1. McFarland, E. W.; Metiu, H., *Chem. Rev.* **2013,** *113* (6), 4391-4427.
2. Ganduglia-Pirovano, M. V.; Hofmann, A.; Sauer, J., *Surf. Sci. Rep.* **2007,** *62* (6), 219-270.
3. West, A. R., *Solid State Chemistry and its Applications, 2nd edition*. John Wiley & Sons, Ltd. : 2013.
4. Jiang, Z.; Chen, S.; Zhang, D., *J. Phys. Chem. C* **2014,** *118* (7), 3789-3794.
5. Kumar, S., *J. Spintron. Magn. Nanomater.* **2012,** *1* (2), 135-138.
6. Lamagna, L.; Molle, A.; Wiemer, C.; Spiga, S.; Grazianetti, C.; Congedo, G.; Fanciulli, M., *J. Electrochem. Soc.* **2012,** *159* (3), H220-H224.
7. Spiga, S.; Rao, R.; Lamagna, L.; Wiemer, C.; Congedo, G.; Lamperti, A.; Molle, A.; Fanciulli, M.; Palma, F.; Irrera, F., *J. Appl. Phys.* **2012,** *112* (1), 014107.
8. Yoo, Y. W.; Jeon, W.; Lee, W.; An, C. H.; Kim, S. K.; Hwang, C. S., *ACS Appl. Mater. Interfaces* **2014,** *6* (24), 22474-22482.
9. Olsen, R. E.; Alam, T. M.; Bartholomew, C. H.; Enfield, D. B.; Woodfield, B. F., *J. Phys. Chem. C* **2014,** *118* (17), 9176-9186.
10. de los Santos, D. M.; Aguilar, T.; Sanchez-Coronilla, A.; Navas, J.; Hernandez, N. C.; Alcantara, R.; Fernandez-Lorenzo, C.; Martin-Calleja, J., *ChemPhysChem* **2014,** *15* (11), 2267-2280.

11.   Islam, M. M.; Bredow, T.; Gerson, A., *Phys. Rev. B* **2007,** *76* (4), 045217.

12.   Shirley, R.; Kraft, M.; Inderwildi, O. R., *Phys. Rev. B* **2010,** *81* (7), 075111.

13.   Iwaszuk, A.; Nolan, M., *J. Phys.-Condes. Matter* **2011,** *23* (33), 334207.

14.   O'Rourke, C.; Bowler, D. R., *J. Phys. Chem. C* **2014,** *118* (14), 7261-7271.

15.   Chiesa, M.; Paganini, M. C.; Giamello, E.; Murphy, D. M.; Di Valentin, C.; Pacchioni, G., *Acc. Chem. Res.* **2006,** *39* (11), 861-867.

16.   Di Valentin, C.; Pacchioni, G., *Acc. Chem. Res.* **2014,** *47* (11), 3233-3241.

17.   Tang, H.; Levy, F.; Berger, H.; Schmid, P. E., *Phys. Rev. B* **1995,** *52* (11), 7771-7774.

18.   Muscat, J.; Wander, A.; Harrison, N. M., *Chem. Phys. Lett.* **2001,** *342* (3-4), 397-401.

19.   Becke, A. D., *J. Chem. Phys.* **1993,** *98* (7), 5648-5652.

20.   Lee, C. T.; Yang, W. T.; Parr, R. G., *Phys. Rev. B* **1988,** *37* (2), 785-789.

21.   Pacchioni, G.; Frigoli, F.; Ricci, D.; Weil, J. A., *Phys. Rev. B* **2001,** *63* (5), 054102.

22.   Nolan, M.; Watson, G. W., *J. Chem. Phys.* **2006,** *125* (14), 144701.

23.   d'Avezac, M.; Calandra, M.; Mauri, F., *Phys. Rev. B* **2005,** *71* (20), 205210.

24.   Gillen, R.; Robertson, J., *Phys. Rev. B* **2012,** *85* (1), 014117.

25.   Weil, J. A.; Bolton, J. R.; Wertz, J. E., *Electron Paramagnetic Resonance*. John Wiley & Sons: New York, 1994.

26.   Chiesa, M.; Giamello, E.; Che, M., *Chem. Rev.* **2010,** *110* (3), 1320-1347.

27.   Stoll, S.; Schweiger, A., *J. Magn. Reson.* **2006,** *178* (1), 42-55.

28.   Dovesi, R.; Orlando, R.; Civalleri, B.; Roetti, C.; Saunders, V. R.; Zicovich-Wilson, C. M., *Z. Kristallogr.* **2005,** *220* (5-6), 571-573.

29.   Dovesi, R.; Saunders, V. R.; Roetti, C.; Orlando, R.; Zicovich-Wilson, C. M.; Pascale, F.; Civalleri, B.; Doll, K.; Harrison, N. M.; Bush, I. J.; D'Arco, P.; Llunell, M., *CRYSTAL09 User's Manual*. University of Torino: Torino, 2009.

30.   Thulin, L.; Guerra, J., *Phys. Rev. B* **2008,** *77* (19), 195112.

31.   Kralik, B.; Chang, E. K.; Louie, S. G., *Phys. Rev. B* **1998,** *57* (12), 7027-7036.

32.   Jain, M.; Chelikowsky, J. R.; Louie, S. G., *Phys. Rev. Lett.* **2011,** *107* (21), 216803.

33.   www.crystal.unito.it.

34.   Lunsford, J. H., *Angew. Chem.-Int. Edit. Engl.* **1995,** *34* (9), 970-980.

35.   Chiesa, M.; Paganini, M. C.; Livraghi, S.; Giamello, E., *Phys. Chem. Chem. Phys.* **2013,** *15* (24), 9435-9447.

36.   Paganini, M. C.; Chiesa, M.; Dolci, F.; Martino, P.; Giamello, E., *J. Phys. Chem. B* **2006,** *110* (24), 11918-11923.

37.   Brown, M.; Primdahl, S.; Mogensen, M., *J. Electrochem. Soc.* **2000,** *147* (2), 475-485.

38.   Brailsford, J. R.; Morton, J. R., *J. Chem. Phys.* **1969,** *51* (11), 4794-4798.

39.   Nuttall, R. H. D.; Weil, J. A., *Solid State Commun.* **1980,** *33* (1), 99-102.

40.   Nuttall, R. H. D.; Weil, J. A., *Can. J. Phys.* **1981,** *59* (12), 1886-1892.

41.   Wertz, J. E.; Auzins, P.; Griffiths, J. H. E.; Orton, J. W., *Discuss. Faraday Soc.* **1959,** *28* (0), 136-141.

42.   Chiesa, M.; Giamello, E.; Di Valentin, C.; Pacchioni, G., *Chem. Phys. Lett.* **2005,** *403* (1-3), 124-128.